Characterization and Synthesis of Duty Cycles for Battery Energy Storage Used in Peak Shaving Dispatch

Kevin Moy
Department of Energy Resource Engineering,
Stanford University,
Stanford, CA 94305
e-mail: kmoy14@stanford.edu

Seong Beom Lee
Department of Energy Resource Engineering,
Stanford University,
Stanford, CA 94305
e-mail: sblee84@stanford.edu

Simona Onori
Department of Energy Resource Engineering,
Stanford University,
Stanford, CA 94305
e-mail: sonori@stanford.edu

Energy storage systems (ESSs), such as lithium-ion batteries, are being used today in renewable grid systems to provide the capacity, power, and quick response required for operation in grid applications, including peak shaving, frequency regulation, back-up power, and voltage support. Each application imposes a different duty cycle on the ESS. This represents the charge/discharge profile associated with energy generation and demand. Different duty cycle characteristics can have different effects on the performance, life, and duration of ESSs. Within lithium-ion batteries, various chemistries exist that own different features in terms of specific energy, power, and cycle life, that ultimately determine their usability and performance. Therefore, the characterization of duty cycles is a key to determine how to properly design lithium-ion battery systems for grid applications. Given the usage-dependent degradation trajectories, this research task is a critical step to study the unique aging behaviors of grid batteries. Significant energy and cost savings can be achieved by the optimal application of lithium-ion batteries for grid-energy storage, enabling greater utilization of renewable grid systems. In this paper, we propose an approach, based on unsupervised learning and frequency domain techniques, to characterize duty cycles for the grid-specific peak shaving applications. Finally, we propose synthetic duty cycles to mimic grid-battery dynamic behaviors for use in laboratory testing. [DOI: 10.1115/1.4050192]

Keywords: dynamics and control, energy storage

1 Introduction

In 2019, global renewable generation capacity reached 2179 GW [1]. While hydropower remains the largest contributor to renewable generation, the fastest-growing resources are photovoltaic and wind power, accounting for 90% of all net renewable capacity additions in 2019. These resources comprise a substantial amount of grid generation power. In California, for example, variable renewable generation (i.e., wind and solar power) constituted 29% of the total generation in 2020 [2]. The introduction of these intermittent generation sources poses challenges to conventional methods for planning the daily operation of the electric grid. Additionally, the diurnal availability of solar generation can aggravate ramping problems when loading increases as solar production decreases. This is problematic in grids with high solar penetration; in the California independent system operator (ISO), this has been termed the "duck curve" [3]. Energy storage systems (ESSs) are considered as a way to address the aforementioned drawbacks. Among many other technologies for ESSs, electrochemical energy storage devices are the main ones implemented and used today for grid services, of which nearly 80% is provided by lithium-ion batteries since 2003 [4,5].

1.1 Motivation. Lithium-ion batteries are prevalent in renewable grid systems since they can provide fast response time, modularity, flexible installation, and short construction periods [6]. ESSs in renewable grid systems participate in applications, such as peak shaving, frequency regulation, voltage support, and back-up power, supporting grid operations at various locations on the grid [7]. However, battery degradation resulting from participation in grid applications is considered a major factor for profitable operation [8]. The degradation trajectories of lithium-ion battery systems depend both on the particular lithium-ion chemistry of the battery and the usage within these grid applications. Current battery technology accounts for various lithium-ion chemistries, each with different characteristics that may be appropriate for different uses within the grid needs. For example, a chemistry with high specific energy but low cycle life may be appropriate for back-up power, as this application only uses the battery during grid outages for extended multi-hour duration [9]. Therefore, properly assessing the most appropriate chemistry for a targeted application can maximize the performance, usability, and duration of entire grid systems.

The usage within each grid application is characterized by duty cycles. A duty cycle is a charge and discharge profile (given in terms of power or current) representing the demands associated with a specific grid application. Understanding degradation mechanisms triggered by characteristic grid-specific duty cycles is a key to developing predictive tools that can be integrated into cost/benefit analyses to maximize revenue and minimize lost capacity. It is well known that differences in duty cycles could significantly impact the durability of ESSs [10]. As the duty cycles and operating conditions can be vastly different for stationary grid-scale storage as opposed to automotive energy storage devices, predictive ESS models properly calibrated over grid-specific duty cycles are missing in today's literature. Moreover, understanding and predicting the performance and durability of large grid-level batteries calls for the study and analysis of actual duty cycles for each application.

In current practice, a plethora of work has been conducted on the analysis and characterization of duty cycles for automotive batteries. In Ref. [11], real driving cycles for hybrid electric vehicles were analyzed by distribution histogram. In Ref. [12], a way of creating effective synthetic duty cycles was published based on pulse-multisine design technique where a discrete Fourier transform

Manuscript received September 30, 2020; final manuscript received February 8, 2021; published online March 16, 2021. Assoc. Editor: Diane L. Peters.

(DFT) approach was adopted to show that the pulse power current duty cycle was insufficient to characterize the amplitude and frequency bandwidth of a real driving cycle. In Ref. [13], real battery duty cycles were categorized by driving speed and style, and an approach based on the power spectral density (PSD) was applied to each category by differentiating discharge and charge events. In addition, various characterization methods have been proposed for different research purposes, using several analytical techniques [14–16]. In Ref. [14], electric bus driving cycles were analyzed using the cross-PSD, involving the DFT of both duty cycles. In Ref. [15], high-performance multisine, random pulse, and inverse cumulative distribution analysis were used to characterize duty cycles of large-format automotive lithium-ion pouch cells. In Ref. [16], a signal design method was proposed to identify battery model parameters using frequency range analysis of actual driving cycles. Current studies in renewable grid applications show the lack of a systematic approach to defining characteristic grid-specific duty cycles. For example, Sandia National Laboratory has previously created a methodology for testing the performance of energy storage, using duty cycles under various grid applications, including peak shaving, frequency regulation, PV smoothing, and solar firming [17]. However, these duty cycles are generated directly from existing data, with the minimal characterization of the duty cycles under this existing data. For PV smoothing, ESS duty cycles were generated from existing PV generation profiles, without identification of characteristic duty cycles [18]. For frequency regulation, PSD was used as an exploratory analysis of the dispatch signal, but ultimately was not used in duty cycle construction; "aggressive" and "average" days from the dispatch were used instead [19].

In other studies, the performance and life of stationary battery systems were investigated, including performance under frequency regulation given different dispatch methodologies [20], and energy arbitrage [8]. These studies adopted simplistic empirical models for battery degradation and predicted performance, and simulated battery degradation directly from the dispatch profiles, without characterizing the dispatch.

In this paper, we first determine characteristic duty cycles using *k-means* clustering for the grid application of peak shaving. We then use the PSD to extract and analyze the frequency content of the clustered duty cycles. The two points above are instrumental for analyzing how grid batteries are operated under this application and can be used to study the unique performance and aging behaviors of batteries in this *modus operandi*.

There are six sections in this paper: peak shaving, methodology, data description, duty cycle analysis, synthetic duty cycles, and conclusions. In Sec. 2, we study and discuss the motivation for and operation of peak shaving, and how battery ESSs are used to support such a grid application. In Sec. 3, we describe in detail fast Fourier transform (FFT), PSD, and k-means clustering, and their relevance to duty cycle analysis. In Sec. 4, we present the data used for the characterization and synthesis of duty cycles. In Sec. 5, we present a method for duty cycle characterization and apply this process to different peak shaving dispatches, and compare them to electric vehicle duty cycles. In Sec. 6, we propose charge/discharge synthetic duty cycles from the cluster centroids study. Concluding remarks are found in the conclusion section. This paper extends upon the previously published work [21].

2 Peak Shaving

The electric utility supplies electricity from the grid to meet the demand of an end user's load, e.g., a house, office, or factory. The facility is then billed monthly by the utility, as measured by the utility meter. The bill charges are defined in a tariff rate determined by the utility and include several elements such as time-of-use charges and demand charges, based on the amount of electric energy and maximum (peak) power consumed from the grid by the load.

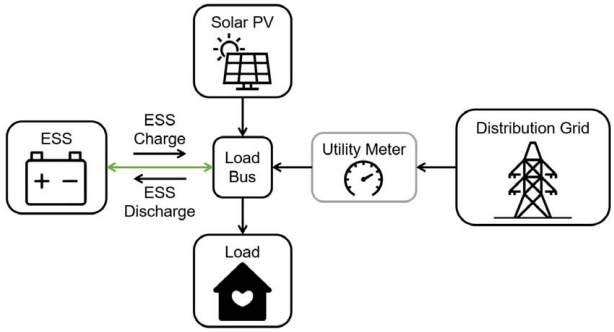

Fig. 1 Peak shaving power flow diagram. Arrows indicate the direction of power flow. The ESS charges and discharges to offset the load, reducing the power flow as seen by the utility meter, and reducing the utility bill.

Peak shaving is used to lower the monthly peak power consumed by the facility from the grid ("shaving" the peak). Different strategies for peak shaving exist, including reducing peak consumption of facility loads, managing the charging of electric vehicles, and dispatching battery ESSs [22]. For battery ESSs, peak shaving is accomplished by discharging when the load is large and charging from the grid when electricity is cheap [23], as shown in Fig. 1. Based on peak shaving, the potential market for residential battery ESSs is approximately 5 million end-users in the United States [24]. Real-time operation of a battery for peak shaving can involve simple control loops to discharge or charge the battery based on current power flow from the grid and state of energy (SOE) of the battery [25] or include an optimization algorithm to compute optimum battery dispatch given additional constraints, such as the power flow through grid infrastructure.

3 Methodology

This section describes the methods and techniques used in this paper to analyze grid application duty cycles.

3.1 Fast Fourier Transform. The DFT of a time-series sequence is calculated by means of FFT method [26]. The DFT takes as input a sequence of values $x[n]$, $n = 0, 1, 2, \ldots, N-1$ of length N, in time. This sequence is then decomposed into a sequence of sinusoidal components $X[q]$, $q = 0, \ldots, N-1$ of length N for different frequencies nq/N.

$$X[q] = \sum_{n=0}^{N-1} x[n] e^{-(i2\pi nq/N)}, \quad q = 0, \ldots, N-1 \tag{1}$$

As described in Sec. 4, the dispatch profiles of the battery are recorded as time-series sequences, so the FFT forms the basis for the duty cycle analysis.

3.2 Mean Centering. The battery dispatches for charging and discharging are strictly negative and strictly positive, respectively. Separating the charge and discharge and directly taking the FFT would yield a bias in the FFT periodogram, appearing as low-frequency components not present in the original dispatch. In order to remove this effect, mean centering is applied to ensure that the resulting separated charge and discharge profiles have zero mean, while preserving all frequency components in these profiles. Mean centering is applied to the entire dispatch profile using the following procedure:

(1) Construct a new profile consisting of only non-negative (non-positive) dispatch.
(2) Find each individual discharge (charge) instance within this new profile, where a discharge (charge) instance is defined

as the battery starting at 0 dispatch, positively (negatively) dispatching, then returning to 0 dispatch.

(3) Construct a new mean-centered discharge (charge) profile by concatenating each discharge (charge) instance with a copy of reversed sign.

We address the stationarity of the mean-centered signals. Stationarity is defined as when statistical properties (e.g., mean, variance, and covariance) of signals are independent of the time framework. Spectral analysis techniques, such as PSD, assume that the time-series signal is stationary, meaning that its properties do not depend on time [27]. With mean centering, the signal has zero mean, and therefore its mean does not depend on time. The autocorrelation function (ACF) can be used to demonstrate stationarity [28], which correlates a signal with a time-shifted copy. Typically, a stationary signal exhibits low autocorrelation as the time shift increases. In our analysis, the ACF implementation xcorr in MATLAB was used to show that the ACF for the mean-centered discharge and charge profiles decay to zero as the autocorrelation shift increases. This shows that the profiles are stationary, and therefore, the PSD can be appropriately calculated for these profiles.

3.3 Power Spectral Density. The PSD is the measure of a signal's power content as a function of its frequency. Our duty cycle analysis uses Welch's method for computing PSD [29]. It is based on the periodogram of the signal, which in turn is based on the DFT of the signal. Welch's method is summarized as follows: a sequence of values $x[n] = 0, 1, 2, \ldots, N-1$, of length N collected at interval periods T, is partitioned into K segments of length M where $M < N-1$ [30]. These segments overlap by an amount S, usually in the range $0.4M \leq S \leq M$.[1]

For each segment $r = 1 \ldots R$, represented as the subset $x[m]$ of the signal where $m = (r-1)S, \ldots, M + (r-1)S - 1$, a windowed DFT $X_r(f)$ is computed at the frequency f with window function[2] w.

$$X_r(f) = \sum_m x[m]w[m]e^{-i2\pi fm} \tag{2}$$

Then, each segment DFT is used to form the segment's modified periodogram value, $P_r(f)$ as follows:

$$P_r(f) = \frac{1}{\sum_{m=0}^{M} w^2[m]} |X_r(f)|^2 \tag{3}$$

Finally, the periodogram values are averaged to obtain Welch's estimate of the PSD.

$$S_x(f) = \frac{1}{R} \sum_{r=1}^{R} P_r(f) \tag{4}$$

We use the pwelch function in MATLAB for Welch's method for PSD, which uses a Hamming window as the default window function. In addition to the signal sequence, pwelch accepts as parameters frequency f, segment length M, and overlap N'. For our analysis, we choose the frequency to be that of the time-series sequence interval ($f = 1/T$) and overlap $N' = M/2$, both of which are within the ranges suggested by [30]. Fixing these parameters leaves us with M as the sole degree-of-freedom, allowing us to determine the amount of smoothing and averaging in Welch's method; as M decreases for fixed N' and f, more periodograms are calculated across shorter segments. Throughout this paper, these parameters are set at $f = 1/3600$ Hz, $M = 48$, and $N' = M/2 = 24$, chosen to balance the tradeoff between smoothing and noise reduction.[3]

[1]This rule of thumb for selecting overlap S is as presented in Ref. [30].

[2]The window function is used to take into account the fact that the segment may not be an exact multiple of a given frequency. The windowing function is greatest in the center of the segment and decreases towards zero at the ends, so that any discontinuities between the beginning and end of the signal are minimized.

[3]The choice of M and N correspond to segments of 2 days and 1 day, respectively.

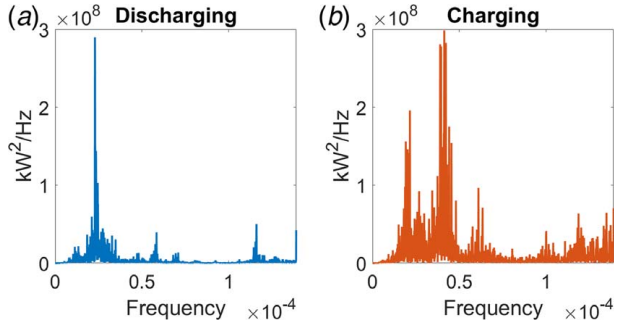

Fig. 2 Periodogram from FFT for peak shaving yearly dispatch "LargeOfficeNew" profile. The FFT and its respective periodogram are computed for the (*a*) discharge and (*b*) charge dispatch profiles, separately.

By averaging these modified (windowed) periodograms, Welch's method for PSD allows us to study the spectral characteristics of a dataset, removing much of the signal noise retained in the FFT. Figure 2 shows the periodogram of the FFT for the peak shaving dispatch profile, separated by charge and discharge. The PSD for the same dispatch profile is also shown in Fig. 13, displaying the same characteristics as the FFT periodogram but with a smoother profile.

As the degradation and health of the battery are dependent on different mechanisms for charging and discharging, separating these two events in the PSD analysis could give useful insights into the battery usage. For example, the Solid Electrolyte Interface (SEI) layer growth has been regarded as one of the main causes of capacity fade and impedance increase in the lithium-ion battery system. The SEI layer will dominantly grow on the anode at every charging event [31]. Lithium plating is also known to occur on the anode when batteries are charged at high rates (or low temperatures). Lithium plating not only causes capacity/power fade but also poses a significant safety concern [32]. Recent works also indicate that lithium plating can also occur at mild charging conditions after extended cycling, leading to rapid aging of the cell [33].

3.4 k-means Clustering. Clustering is an unsupervised learning method to organize and partition data into "clusters." Data within each cluster share some features [34]. This class of methods has been widely studied for characterizing time-series data [35].

In k-means clustering, k clusters are constructed from n observations of data, where each observation is assigned a cluster by the closest Euclidean distance to the cluster centroid, or the mean value of all observations in the cluster. That is, given k desired clusters, and dataset of observations $x_1 \ldots x_n$, k-means clustering determines k cluster centroids as a solution $\phi^* = [c_1 \ldots c_k]^T$ that minimizes the cost function J [36] as

$$\phi^* = \min J \tag{5}$$

$$J = \sum_{i=1}^{n} \min_{j=1 \ldots k} x_i - c_j^2 \tag{6}$$

We use the k-means function in MATLAB to apply k-means clustering to the dispatch profiles. As the initialization of the cluster centroids is important for clustering convergence, the k-means++ algorithm is used for this initialization [36]. Within the context of electric power systems, k-means clustering has been applied to solar and wind generation profiles [37,38], electricity load demand profiles [39,40], and driving cycles for electric vehicles [41]. This paper represents the first application of k-means clustering to grid storage battery dispatch profiles. The application of k-means clustering to the dataset is as follows. We first choose

each observation to represent 1 day, reshaping the time-series data into an array where each row is the dispatch for 1 day, and each column is the dispatch for 1 h within the day. Next, as some days contain zero dispatch (i.e., no charging or discharging of the battery), the corresponding rows of the array are removed. Days with missing or corrupted values (e.g., NaN) are also removed. The number of clusters, k, is then chosen, and k-means clustering is applied to the remaining nonzero dispatch array.

The output of k-means clustering on the dispatch data is k "cluster centroids," representing the average daily dispatch within each cluster, and cluster assignments for each nonzero dispatch day.

4 Data Description

The time-series dispatch profiles for the grid application are summarized in Table 1. Peak shaving data were obtained from a publicly available optimization and simulation tool for energy storage: QuESt, developed by Sandia National Laboratories [42]. QuESt allows users to select facility load profiles, energy storage parameters such as rated power and energy, as well as a tariff rate structure. QuESt then uses this input data to simulate the energy storage dispatch per month over 1 year, optimizing the dispatch for bill reduction by peak shaving. This dispatch data is obtained as an hourly dispatch (frequency 1/3600 Hz).

Figure 3 shows the QuESt-simulated dispatch of the 200 kW, 400 kWh battery using the "LargeOfficeNew" load over the year. The histogram in Fig. 4(*a*) shows a bias toward high-power charging of the battery. The histogram in Fig. 4(*b*) also shows that when the battery is at rest (i.e., neither charging nor discharging), the majority of rest instances are less than 48 h in length, with most rest instances between 10 and 20 h long. These rest instances are periods of time when the battery is not actively used for peak shaving and indicate opportunities to employ the batteries for other grid applications during these periods.

Figure 5 shows the QuESt-simulated dispatch of the 200 kW, 400 kWh battery using the "SuperMarketNew" load over the year. Figure 6 is the histogram of nonzero dispatch over the year for the "SuperMarketNew" load, showing that there is both a different distribution of charging and discharging, as well as more frequent dispatch with shorter rest periods, compared to the "LargeOfficeNew" load.

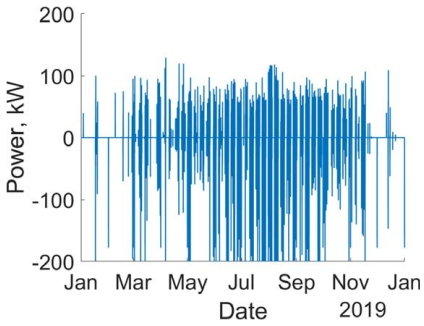

Fig. 3 Yearly dispatch of a 200 kW, 400 kW grid storage battery for peak shaving, "LargeOfficeNew" profile. The QuESt tool was used to produce this dispatch, which QuESt simulated on an hourly basis. Discharging is positive, while charging is negative.

Table 1 Grid application dispatch data sources

Application	System rated power, kw	System rated energy, kwh	Load name	Tariff rate
Peak Shaving	200	400	LargeOfficeNew	PG&E E19
			SuperMarketNew	PG&E A10

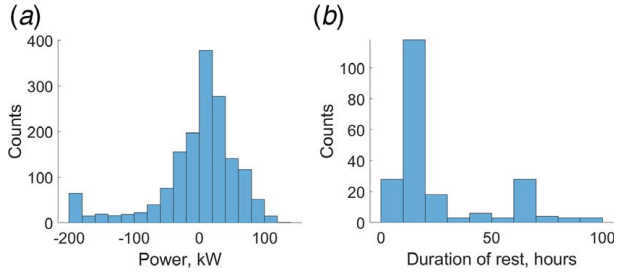

Fig. 4 (*a*) Histogram of nonzero peak shaving dispatch, "LargeOfficeNew." Datapoints corresponding to zero dispatch were excluded from this histogram. Histogram shows a bias toward higher charging (negative) power. (*b*) Histogram of rest periods during dispatch, "LargeOfficeNew." The period of rest is determined as the length of time between when a charge or discharge ends, and the next charge or discharge begins.

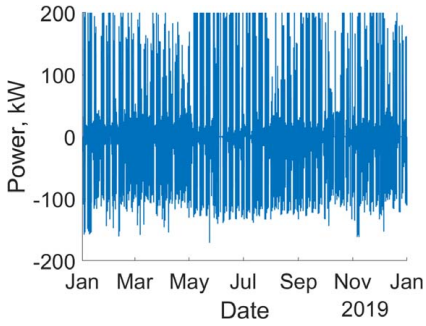

Fig. 5 Yearly dispatch of a 200 kW, 400 kW grid storage battery for peak shaving, "SuperMarketNew" profile. The QuESt tool was used to produce this dispatch on hourly basis. Discharging is positive, while charging is negative.

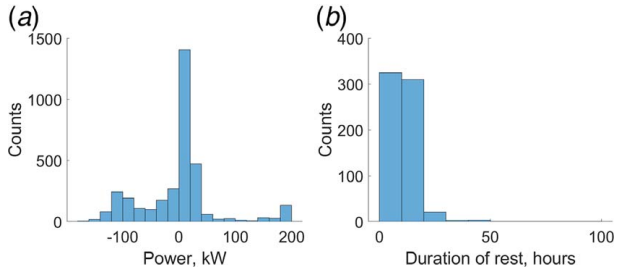

Fig. 6 (*a*) Histogram of nonzero peak shaving dispatch, "SuperMarketNew." Datapoints corresponding to dispatch of 0 were excluded from this histogram. (*b*) Histogram of rest periods during dispatch, "SuperMarketNew." The period of rest is determined as the length of time between when a charge or discharge ends, and the next charge or discharge begins.

5 Duty Cycle Analysis

For a given grid storage application dispatch profile, we conduct the following steps. First, we use k-means clustering to obtain distinct duty cycle clusters. The number of clusters is chosen to determine duty cycles that represent the range of charging and discharging behavior within the dispatch profile under consideration. Then, within each cluster, we compute the PSD of the charge and discharge separately. This process is summarized in Fig. 7.

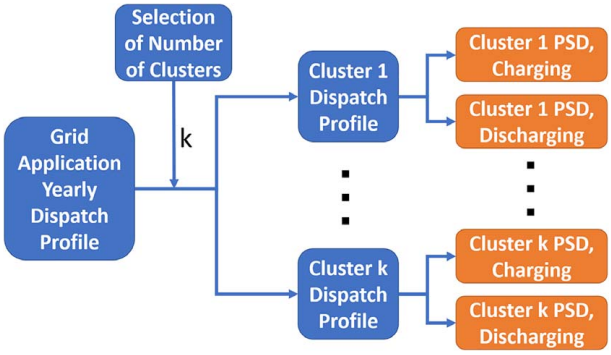

Fig. 7 Flow diagram for duty cycle analysis. The outputs of this analysis are shown at right: the PSD computed for charging and discharging within each dispatch cluster, for all *k* clusters.

5.2 LargeOfficeNew Load Peak Shaving Dispatch. This section applies the analysis described in Fig. 7 to the peak shaving dispatch profile simulated by QuESt for the "LargeOfficeNew" facility load.

5.2.1 Selection of Number of Clusters. Previous studies of residential facility load have revealed the differences in load between seasons [40]. As peak shaving dispatch is dependent on facility load, we conduct a seasonal analysis of the peak shaving dispatch to choose the number of clusters, k. We divide this dispatch into four seasonal events as follows:

(i) Spring: March, April, May
(ii) Summer: June, July, August
(iii) Fall: September, October, November
(iv) Winter: December, January, February

Figure 8 shows the histogram of peak shaving dispatch on the "LargeOfficeNew" load for each season. We find that a majority of dispatch occurs in the summer, with limited activity in the winter and roughly equivalent dispatch distribution in the spring and fall. We also evaluate the differences in charging across seasons. This is shown in Fig. 9; there are only 19 charging instances during the winter season, while all other seasons have at least 80. Based on the seasonal analysis, there appears to be an active dispatch segment of the year (summer), followed by a section of the year of moderate dispatch activity (spring and fall), and a section of mild dispatch (winter). We choose a value for

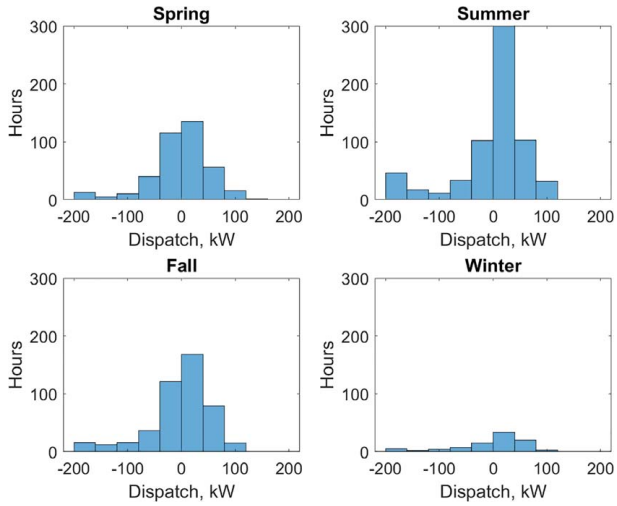

Fig. 8 Histogram of nonzero peak shaving dispatch by season, "LargeOfficeNew"

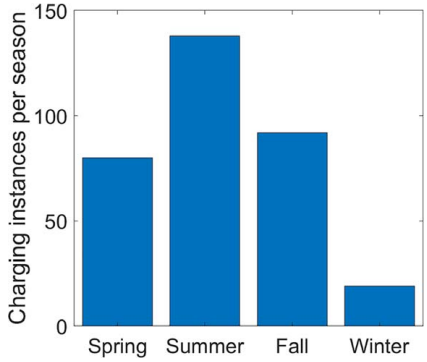

Fig. 9 Charging instances by season, "LargeOfficeNew"

$k = 2$ for k-means clustering, to cluster the dispatch between the active dispatch and the moderate/mild dispatch, and then characterize the duty cycle within each cluster.

5.1.2 Clustering Analysis. Using the methodology for k-means described in Sec. 3.4 with $k = 2$, we obtain two clusters, Cluster 1 and Cluster 2. Figure 10 is the assignment of clusters for each nonzero dispatch day throughout the year. Day assignments for Cluster 1 fall mainly in the summer, and day assignments for Cluster 2 fall mainly in the remainder of the year.

The two clusters have respective centroids, here interpreted as a representative daily dispatch of the battery within each cluster. Figure 11 shows the two cluster centroids, with Centroid 1 as the centroid for cluster 1 and Centroid 2 as the centroid for cluster 2. It is from this figure that the underlying operating protocol for peak shaving dispatch in QuESt can be seen: the dispatch charges the battery immediately before the discharge required for peak

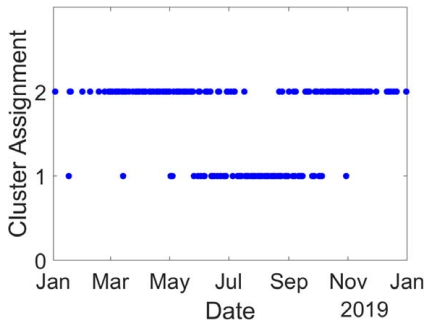

Fig. 10 Cluster assignments for each day of yearly dispatch. "LargeOfficeNew." Days without charge or discharge (zero-dispatch days) are not assigned a cluster.

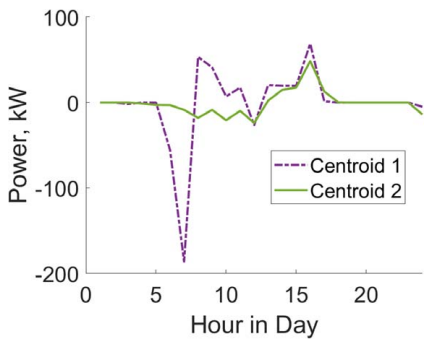

Fig. 11 Cluster centroids of yearly dispatch, "LargeOfficeNew." Cluster centroids as determined by k-means clustering on the yearly dispatch, cluster length 1 d = 24 h.

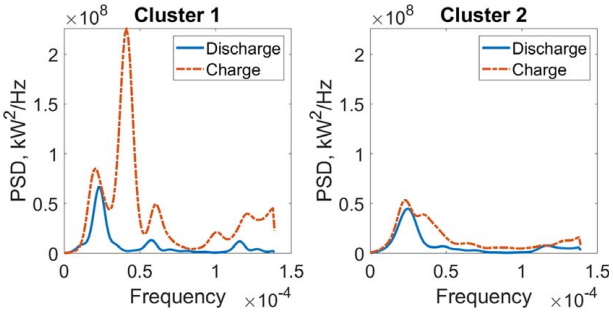

Fig. 12 Power spectral density of peak shaving dispatch, "LargeOfficeNew," by Cluster. PSD was conducted on clusters within the yearly dispatch, as assigned in Fig. 10.

shaving. As Centroid 1 requires a longer discharge than Centroid 2, the charging beforehand is at much higher power to fill the battery, in anticipation of a higher energy discharge.

We now compute the PSD for charge and discharge separately of the two clusters, with mean centering applied as described in Sec. 3.3. Figure 12 shows the PSD computed for charging and discharging for each cluster. The PSD computed for Cluster 1 charging exhibits a strong peak at 4.123e−05 Hz, while the PSD as computed for Cluster 2 charging shows a much smaller peak at 2.279e−05 Hz. For discharging, the PSD computed for Cluster 1 and Cluster 2 exhibits peaks of similar size, at 2.279e−05 Hz and 2.496e −05 Hz, respectively, showing that the frequency content of the discharge between clusters is comparable.

5.1.3 Comparison to Power Spectral Density Computed Over Entire Dispatch. We compute now the PSD over the entire year without k-means clustering. This is presented in Fig. 13. The PSD computed for charging contains a strong peak at 4.015e −5 Hz, and in the PSD computed for discharging, a peak at 2.387e−5 Hz. These are closer in value to those of Cluster 1, than those of Cluster 2. The PSD computed over the entire year is dominated by the charging profile in Cluster 1. However, Cluster 1 only represents 27% of the total nonzero dispatch days. Characterizing the peak-shaving dispatch duty cycle based on the yearly PSD would obscure the characteristic duty cycling of Cluster 2.

5.2 SuperMarketNew Load Peak Shaving Dispatch. This section applies the analysis described in Fig. 7 to the peak shaving dispatch profile simulated by QuESt for the "SuperMarketNew" facility load, and compares the results of this analysis to that of the "LargeOfficeNew" facility load.

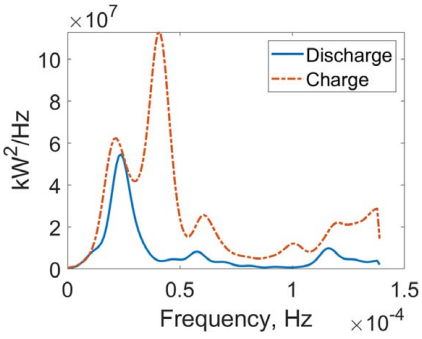

Fig. 13 Power spectral density of peak shaving yearly dispatch, "LargeOfficeNew." The charging PSD exhibits a strong peak at 4.015e−5 Hz, while the discharging PSD exhibits a peak at 2.387e−5 Hz.

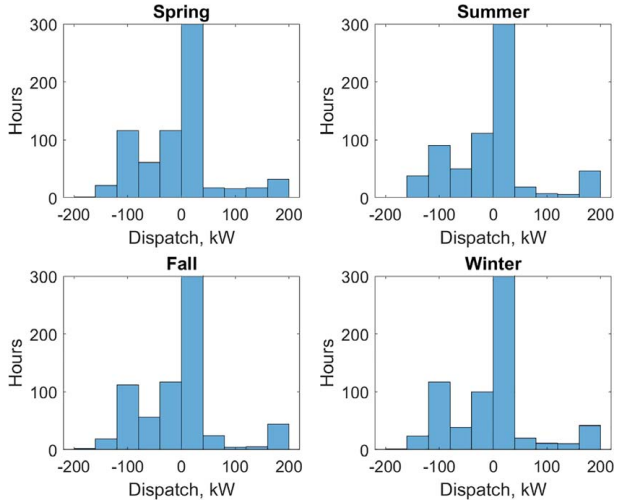

Fig. 14 Histogram of nonzero peak shaving dispatch by season, "SuperMarketNew"

5.2.1 Selection of Number of Clusters. For the "SuperMarketNew" load, Fig. 14 is the histogram for peak shaving dispatch profile on that load within each season, and Fig. 15 is the instances of charging occurrences by season, displaying more consistent dispatch across seasons than for the "LargeOfficeNew" dispatch profile. Unlike with the "LargeOfficeNew" dispatch profile, we cannot rely on seasonal differences in a dispatch to inform the selection of a number of clusters for the "SuperMarketNew" dispatch profile.

We instead choose the number of clusters so that applying k-means clustering to the dispatch profile yields clusters of comparable sizes to avoid over-generalizing the dispatch and clustering the majority of daily dispatch into a given cluster. For this dispatch profile, using $k=2$ yields one cluster with 344 days and one cluster with only 15 days. Using $k=3$ yields three clusters of sizes 145, 113, and 101 days. We adopt this choice.

5.2.2 Clustering Analysis. Using the methodology for k-means described in Sec. 3.4 with $k=3$, we obtain three clusters, Cluster 1, Cluster 2, and Cluster 3. Figure 16 is the assignment of clusters for each nonzero dispatch day throughout the year. As expected from our seasonal analysis on this dispatch profile, clusters do not appear to correspond to any seasonal dispatch.

The three clusters have respective centroids, here interpreted as a representative daily dispatch of the battery within each cluster. Figure 17 shows the three cluster centroids, with Centroid 1 as the centroid for cluster 1, Centroid 2 as the centroid for cluster 2, and Centroid 3 as the centroid for cluster 3. There are three distinct dispatch profiles: Centroid 1 represents days with a medium charge

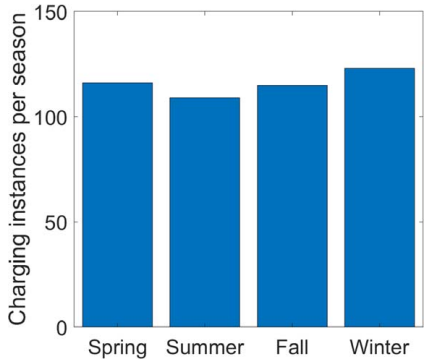

Fig. 15 Charging instances by season, "SuperMarketNew"

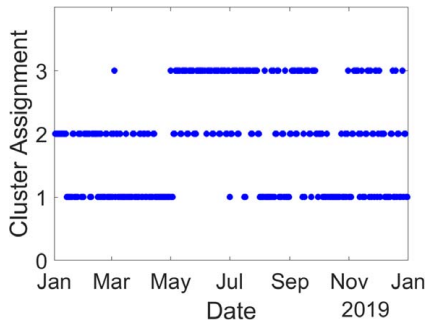

Fig. 16 Cluster assignments for each day of yearly dispatch, "SuperMarketNew." Days without charge and discharge (zero-dispatch days) are not assigned a cluster.

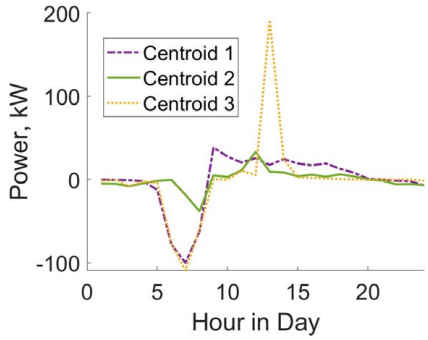

Fig. 17 Cluster centroids of yearly dispatch, "SuperMarketNew." Cluster centroids as determined by k-means clustering on the yearly dispatch, cluster length 1 d = 24 h.

power and low discharge power; Centroid 2 represents days with a low charge and discharge power; and Centroid 3 represents days with a medium charge and high discharge power.

The PSD for charge and discharge of the three clusters is computed, with mean centering applied as in Sec. 3.3. Figure 18 shows the PSD computed for charging and discharging for each cluster. Cluster 1 shows a strong peak in the PSD computed for charging, at 2.713e−5 Hz. Cluster 2 shows no discernable peaks in the PSD computed for charging and discharging. Cluster 3 shows peaks in the PSD computed for charging at 2.713e−5 Hz, the same as in Cluster 1, and a large peak in the PSD computed for discharging at 1.378e−4 Hz, representing the high-power, short-duration discharge observed within that cluster, as seen in Centroid 3.

5.2.3 Comparison to Power Spectral Density Computed Over Entire Dispatch. As in Sec. 5.1.3, we also compute the PSD over the entire year, without k-means clustering, for the "SuperMarketNew" dispatch profile. This is shown in Fig. 19. The PSD computed for charging shows a peak at 2.604e−5 Hz, and no discernable peak for discharging. In this case, many of the duty cycling features present in the "SuperMarketNew" clusters are missing, including the large peak in the PSD computed for Cluster 3 discharging, which are important to characterize the calendar cycling during this dispatch.

5.3 Comparison to Electric Vehicle Duty Cycles. Table 2 compares the frequency corresponding to the peak value of the PSD for peak shaving to those obtained by Liu et al. in Ref. [13], which evaluated simulated 48 V "mild-hybrid" vehicle battery dispatch using PSD. These values are also compared to the same values obtained for the simulated dispatch of a Tesla Model S "fully-electric" vehicle battery, on the US06 and WLTP driving

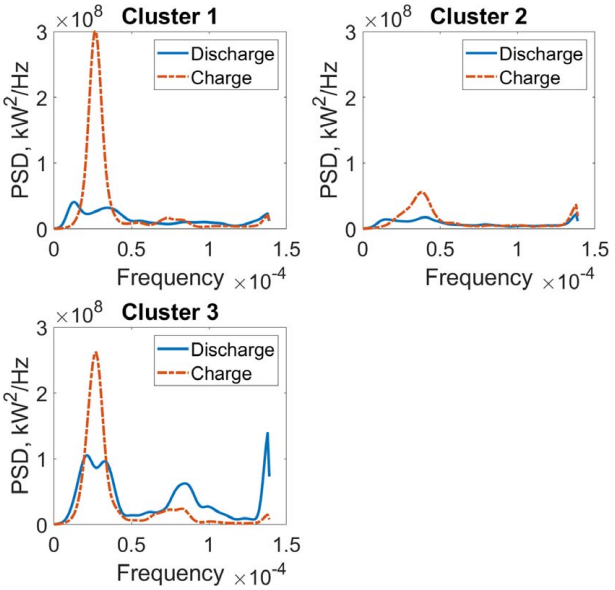

Fig. 18 Power spectral density of peak shaving dispatch, "LargeOfficeNew," by Cluster. PSD was conducted on clusters within the yearly dispatch, as assigned in Fig. 16.

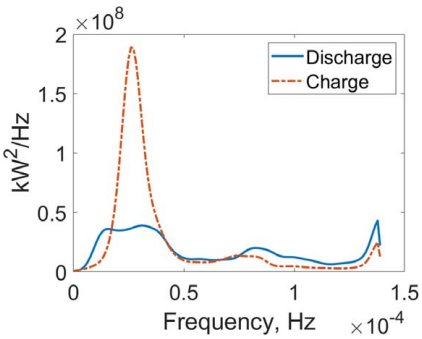

Fig. 19 Power spectral density of peak shaving yearly dispatch, "SuperMarketNew." The charging PSD exhibits a strong peak at 2.604e−5 Hz, while there is no discernable peak in discharge.

cycles. The "LargeOfficeNew" and "SuperMarketNew" yearly dispatches are chosen as representatives for peak shaving.

With the exception of the mild-hybrid vehicle discharge, the peak frequency of the PSD for peak shaving is at least two orders of magnitude smaller than that of the PSD for the batteries in automotive applications. Batteries for grid applications are excited across a different frequency range, and therefore exhibit different impedances, than in automotive applications. This difference could have implications on the design of battery management systems (BMS) for grid batteries in comparison to electric automotive batteries.

This difference also has implications on the operation of second-life batteries (i.e., post-automotive-usage) for grid applications. As a

Table 2 PSD peak frequencies by application

Application	Discharge PSD peak frequency, Hz	Charge PSD peak frequency, Hz
Peak Shaving, "LargeOfficeNew"	2.39e−5	4.02e−5
Peak Shaving, "SuperMarketNew"	2.60e−5	1.38e−4
Mild-Hybrid Vehicle [13]	4e−4–1.17e−2	3.52e−2–4.69e−2
Fully-Electric Vehicle, US06	7.81e−3	4.69e−2
Fully-Electric Vehicle, WLTP	1.56e−2	1.95e−2

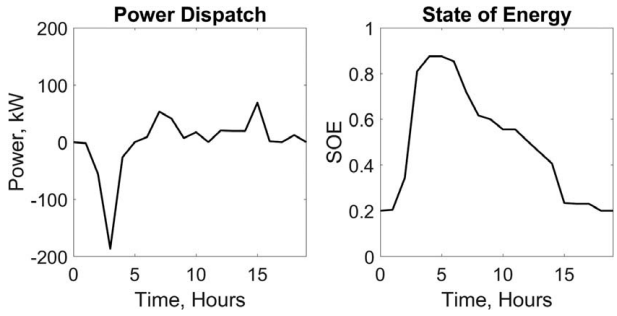

Fig. 20 Synthetic duty cycle for the peak shaving dispatch, "LargeOfficeNew." Cluster Centroid 1 from Fig. 11 is used to create the (*a*) synthetic duty cycle power dispatch, with (*b*) resulting variation of SOE.

second-life battery is excited across a different frequency range, its degradation within grid application operation will be different than in its "first-life" in electric vehicle operation. Therefore, models to estimate degradation and capacity fade for the electric vehicle operation will likely not be accurate for the grid application operation, and new tuning could be necessary for the new grid operation mode.

6 Synthetic Duty Cycles

Accurately estimating capacity fade of the battery system is a key element to maximize its usability and lifetime in stationary grid applications. Battery aging can be categorized into two types: cycling and calendar aging [43]. Batteries undergo cycling aging when they are charged or discharged. The cycling aging is mainly affected by the charging/discharging pattern characteristics. In lithium-ion batteries, capacity fade caused by cycling occurs due to unwanted side reactions, such as SEI layer formation, lithium plating at the negative electrode, and intercalation-induced stresses [44]. Calendar aging is independent of charge–discharge cycling; it occurs when the batteries are at rest. Calendar aging is an important factor in grid applications when the resting period is substantial or not negligible, compared to charging/discharging events [43].

The cluster centroids are used as the basis for synthetic representations of the yearly duty cycle. Figure 20(*a*) shows the proposed synthetic duty cycle for the "LargeOfficeNew" dispatch. The synthetic duty cycle is created based on Centroid 1, thereby removing the redundant dispatch information in the two cluster centroids in Fig. 11. Given its high-power charge, it covers the full range of power of the dispatch duty cycling and characterizes the worst-case scenario.

The synthetic duty cycle includes the high-power charge cycle and then two lower-power discharge cycles derived from Centroid 1 dispatch. It then includes a small, low-power discharge in order to ensure that the duty cycle is energy-neutral (i.e., the battery starts and ends at the same SOE). This is shown in Fig. 20(*b*) for a starting SOE of 0.2. The SOE reaches a maximum of 0.875 during the synthetic duty cycle, then returns to 0.2 after completing the synthetic duty cycle.

The synthetic duty cycle is confirmed to shorten the yearlong dispatch profile (a total of 8760 h) to 18 h. A rest period of zero-power dispatch can be appended to the synthetic duty cycle to account for calendar aging as well, at the expense of extending the length of the duty cycle.

7 Conclusions

A process for characterizing the duty cycle of grid applications for energy storage was presented, using k-means clustering and PSD for stationary battery under peak shaving applications. The combination of k-means clustering and PSD analysis captures features within each cluster that would otherwise be lost in a PSD analysis conducted over the entire dispatch profile. This process also characterizes the variation in duty cycle within a peak shaving dispatch profile. This allows for direct comparison between peak shaving dispatch profiles, as well as to other applications, such as batteries in mild-hybrid and fully-electric vehicle applications.

The proposed method leads to the design of lab-prone synthetic duty cycles. The developed duty cycles can be used to cycle different chemistries (e.g., Lithium–Iron–Phosphate, Nickel–Manganese–Cobalt, Nickel–Cobalt–Aluminum) to collect degradation data that can be used for long term grid-energy storage analysis. The characterization method can also be applied to analyze other grid storage applications such as frequency regulation, back-up power, and voltage support.

Acknowledgment

The research presented within this paper is supported by the Bits and Watts Initiative within the Precourt Institute for Energy at Stanford University.

Conflict of Interest

There are no conflicts of interest.

References

[1] IRENA, 2020, "Renewable Capacity Highlights," IRENA, Technical Report.
[2] NREL, 2020, "2018 Renewable Energy Grid Integration Data Book," U.S. Department of Energy, Technical Report, https://www.nrel.gov/docs/fy20osti/74823.pdf
[3] California ISO, 2013, "What the Duck Curve Tells us About Managing a Green Grid," California ISO, Technical Report, https://www.caiso.com/Documents/FlexibleResourcesHelpRenewables_FastFacts.pdf
[4] EIA, 2018, "U.S. Battery Storage Market Trends: May 2018," U.S. Energy Information Administration, Technical Report.
[5] Lazard, 2017, "Lazard's Levelized Cost of Storage Analysis—version 3.0," Lazard, Technical Report.
[6] Chen, T., Jin, Y., Lv, H., Yang, A., Liu, M., Chen, B., Xie, Y., and Chen, Q., 2020, "Applications of Lithium-Ion Batteries in Grid-Scale Energy Storage Systems," Transactions of Tianjin University, **26**, pp. 208–217.
[7] Rocky Mountain Institute, 2015, "The Economics of Battery Energy Storage," Rocky Mountain Institute, Technical Report, https://rmi.org/insight/economics-battery-energy-storage/
[8] Wankmüller, F., Thimmapuram, P. R., Gallagher, K. G., and Botterud, A., 2017, "Impact of Battery Degradation on Energy Arbitrage Revenue of Grid-Level Energy Storage," J. Energy Storage, **10**, pp. 56–66.
[9] Stan, A., Świerczyński, M., Stroe, D., Teodorescu, R., and Andreasen, S. J., 2014, "Lithium Ion Battery Chemistries From Renewable Energy Storage to Automotive and Back-up Power Applications—An Overview," 2014 International Conference on Optimization of Electrical and Electronic Equipment, pp. 713–720.
[10] Crawford, A. J., Huang, Q., Kintner-Meyer, M. C. W., Zhang, J.-G., Reed, D. M., Sprenkle, V. L., Viswanathan, V. V., and Choi, D., 2018, "Lifecycle Comparison of Selected Li-ion Battery Chemistries Under Grid and Electric Vehicle Duty Cycle Combinations," J. Power Sources, **380**, pp. 185–193.
[11] Spagnol, P., Onori, S., Madella, N., Guezennec, Y., and Neal, J., 2010, "Aging and Characterization of li-ion Batteries in a hev Application for Lifetime Estimation," Proceedings of the IFAC Symposium Advances in Automotive Control.
[12] Widanage, W., Barai, A., Chouchelamane, G. H., Uddin, K., McGordon, A., Marco, J., and Jennings, P., 2016, "Design and use of Multisine Signals for Li-ion Battery Equivalent Circuit Modelling. Part 1: Signal Design," J. Power Sources, **324**, pp. 70–78.
[13] Liu, Z., Onori, S., and Ivanco, A., 2017, "Synthesis and Experimental Validation of Battery Aging Test Profiles Based on Real-World Duty Cycles for 48-V Mild Hybrid Vehicles," IEEE Trans. Veh. Technol., **66**(10), pp. 8702–8709.
[14] Mingant, R., Bernard, J., and Sauvant-Moynot, V., 2016, "Novel State-of-Health Diagnostic Method for Li-ion Battery in Service," Appl. Energy, **183**, pp. 390–398.
[15] Kellner, Q., Worwood, D., Barai, A., Widanage, W. D., and Marco, J., 2018, "Duty-cycle Characterisation of Large-Format Automotive Lithium ion Pouch Cells for High Performance Vehicle Applications," J. Energy Storage, **19**, pp. 170–184.
[16] Zhu, R., Duan, B., Zhang, C., and Gong, S., 2019, "Accurate Lithium-ion Battery Modeling With Inverse Repeat Binary Sequence for Electric Vehicle Applications," Appl. Energy, **251**, p. 113339.

[17] Conover, D. R., 2016, "Protocol for Uniformly Measuring and Expressing the Performance of Energy Storage Systems," United States, https://www.osti.gov/servlets/purl/1249270, Accessed January 4, 2016.
[18] Schoenwald, D. A., and Ellison, J., 2016, "Determination of Duty Cycle for Energy Storage Systems in a PV Smoothing Application," United States, https://www.osti.gov/servlets/purl/1331494
[19] Rosewater, D., and Ferreira, S., 2016, "Development of a Frequency Regulation Duty-Cycle for Standardized Energy Storage Performance Testing," https://www.osti.gov/servlets/purl/1257783
[20] Stroe, D., Knap, V., Swierczynski, M., Stroe, A., and Teodorescu, R., 2017, "Operation of a Grid-Connected Lithium-Ion Battery Energy Storage System for Primary Frequency Regulation: A Battery Lifetime Perspective," IEEE Trans. Ind. Appl., **53**(1), pp. 430–438.
[21] Moy, K., Lee, S. B., and Onori, S., "Characterization of Duty Cycles for the Peak Shaving Electric Grid Energy Storage Application," Presented at the ASME 2020 Dynamic Systems and Control Conference, Pittsburgh, PA, Oct. 4–7, 2020.
[22] Uddin, M., Romlie, M. F., Abdullah, M. F., Abd Halim, S., Abu Bakar, A. H., and Chia Kwang, T., 2018, "A Review on Peak Load Shaving Strategies," Renewable Sustainable Energy Rev., **82**, pp. 3323–3332.
[23] End-User Bill Management, 2013, "*Energy Storage Association*, https://energystorage.org/end-user-bill-management/
[24] NREL, 2017, "Identifying Potential Markets for Behind-the-Meter Battery Energy Storage: A Survey of U.S. Demand Charges," U.S. Department of Energy, Technical Report, https://www.nrel.gov/docs/fy17osti/68963.pdf
[25] Leadbetter, J., and Swan, L., 2012, "Battery Storage System for Residential Electricity Peak Demand Shaving," Energy Build., **55**, pp. 685–692.
[26] Cooley, J. W., Lewis, P. A. W., and Welch, P. D., 1969, "The Fast Fourier Transform and Its Applications," IEEE Trans. Educ., **12**(1), pp. 27–34.
[27] Hyndman, R. J., and Athanasopoulos, G., 2018, *Forecasting: Principles and Practice*, OTexts: Melbourne, Australia.
[28] Lee, D., and Baldick, R., 2012, "Analyzing the Variability of Wind Power Output Through the Power Spectral Density," 2012 IEEE Power and Energy Society General Meeting.
[29] Welch, P., 1967, "The use of Fast Fourier Transform for the Estimation of Power Spectra: A Method Based on Time Averaging Over Short, Modified Periodograms," IEEE Trans. Audio Electroacoust., **15**(2), pp. 70–73.
[30] Sandia National Labs, 1991, "PSD Computations Using Welch's Method," U.S. Department of Energy, Technical Report, https://www.osti.gov/biblio/5688766/
[31] Ramadass, P., Haran, B., Gomadam, P. M., White, R., and Popov, B. N., 2004, "Development of First Principle Capacity Fade Model for Li-Ion Cells," J. Electrochem. Soc., **151**(2), pp. A196–A203.
[32] Liu, Q., Du, C., Shen, B., Zuo, P., Cheng, X., Ma, Y., Yin, G., and Gao, Y., 2016, "Understanding Undesirable Anode Lithium Plating Issues in Lithium-ion Batteries," RSC Adv., **6**(91), pp. 88683–88700.
[33] Yang, X. G., Leng, Y., Zhang, G., Ge, S., and Wang, C. Y., 2017, "Modeling of Lithium Plating Induced Aging of Lithium-ion Batteries: Transition From Linear to Nonlinear Aging," J. Power Sources, **360**, pp. 28–40.
[34] Jain, A. K., Murty, M. N., and Flynn, P. J., 1999, "Data Clustering: a Review," ACM Comput. Surv., **31**(3), pp. 264–323.
[35] Warren Liao, T., 2005, "Clustering of Time Series Data—a Survey," Pattern Recognit., **38**(11), pp. 1857–1874.
[36] Arthur, D., and Vassilvitskii, S., 2007, "k-means++: the Advantages of Careful Seeding," Presented at the Proceedings of the Eighteenth Annual ACM-SIAM Symposium on Discrete Algorithms, New Orleans, LA.
[37] Xu, T., and Zhang, N., 2017, "Coordinated Operation of Concentrated Solar Power and Wind Resources for the Provision of Energy and Reserve Services," IEEE Trans. Power Syst., **32**(2), pp. 1260–1271.
[38] Deeba, S. R., Sharma, R., Saha, T. K., and Chakraborty, D., 2015, "A Tool to Estimate Maximum Arbitrage From Battery Energy Storage by Maintaining Voltage Limits in an LV Network," IEEE PES Asia-Pacific Power and Energy Engineering Conference (APPEEC), pp. 1–5.
[39] Green, R., Staffell, I., and Vasilakos, N., 2014, "Divide and Conquer? *k*-Means Clustering of Demand Data Allows Rapid and Accurate Simulations of the British Electricity System," IEEE Trans. Eng. Manage., **61**(2), pp. 251–260.
[40] Rhodes, J. D., Cole, W. J., Upshaw, C. R., Edgar, T. F., and Webber, M. E., 2014, "Clustering Analysis of Residential Electricity Demand Profiles," Appl. Energy, **135**, pp. 461–471.
[41] Devie, A., Montaru, M., Pelissier, S., and Venet, P., 2010, "Classification of Duty Pulses Affecting Energy Storage Systems in Vehicular Applications," IEEE Vehicle Power and Propulsion Conference, pp. 1–6.
[42] Sandia National Labs, 2018, "QuESt: An Energy Storage Evaluation Application Suite," U.S. Department of Energy, https://www.sandia.gov/ess-ssl/tools/quest/
[43] Smith, K., Saxon, A., Keyser, M., Lundstrom, B., Cao, Z., and Roe, A., 2017, "Life Prediction Model for Grid-Connected Li-ion Battery Energy Storage System," 2017 American Control Conference (ACC).
[44] Reniers, J. M., Mulder, G., and Howey, D. A., 2019, "Review and Performance Comparison of Mechanical-Chemical Degradation Models for Lithium-Ion Batteries," J. Electrochem. Soc., **166**(14), A3189–A3200.